DOI: 10.1002/ ((please add manuscript number))
Article type: Full Paper

Self-Assembled Metal–Phenolic Networks on Emulsions as Low-Fouling and pH-Responsive Particles

*Quinn A. Besford, Yi Ju, Ting-Yi Wang, Gyeongwon Yun, Pavel Cherepanov, Christoph E. Hagemeyer, Francesca Cavalieri, and Frank Caruso**

Dr. Q. A. Besford, Dr. Y. Ju, Dr. G. Yun, Dr. P. Cherepanov,[+] Dr. F. Cavalieri, Prof. F. Caruso
ARC Centre of Excellence in Convergent Bio-Nano Science and Technology, and the Department of Chemical Engineering, The University of Melbourne, Parkville, Victoria 3010, Australia
E-mail: fcaruso@unimelb.edu.au

Dr. T.-Y Wang, A./Prof. C. E. Hagemeyer
NanoBiotechnology Laboratory, Australian Centre for Blood Diseases, Monash University, Victoria 3004, Australia

[+] Current address: Centre for Advanced 2D Materials, National University of Singapore, Singapore

Keywords: self-assembly, metal–phenolic networks, emulsion, drug delivery, nanomaterials

Interfacial self-assembly is a powerful organizational force for fabricating functional nanomaterials, including nanocarriers, for imaging and drug delivery. Herein, we report the interfacial self-assembly of pH-responsive metal–phenolic networks on the liquid–liquid interface of oil-in-water emulsions. Oleic acid emulsions of 100–250 nm in diameter are generated by ultrasonication, to which poly(ethylene glycol) (PEG)-based polyphenolic ligands are assembled with simultaneous crosslinking by metal ions, thus forming an interfacial metal–phenolic network (MPN). PEG provides a protective barrier on the emulsion phase and renders the emulsion low fouling. The MPN-coated emulsions have a similar size and dispersity, but an enhanced stability when compared with the raw emulsions, and exhibit a low cell association in vitro, a blood circulation half-life of ca. 48 min in vivo, and are nontoxic to healthy mice. Furthermore, a model anticancer drug, doxorubicin, can be encapsulated within the emulsion phase at a high loading capacity (~5 fg of doxorubicin per emulsion). The MPN coating imparts pH-responsiveness to the drug-loaded emulsions, leading to drug release at cell internalization pH and a potent cell cytotoxicity. Our

results highlight a straightforward strategy for the interfacial nanofabrication of pH-responsive emulsion–MPN systems with potential use in biomedical applications.

1. Introduction

The development of functional nanomaterials is vital in the field of nanomedicine, where nanomaterials play a key role in efficiently carrying and selectively delivering therapeutic agents for the treatment of disease.[1,2] Self-assembly, a process that allows simple molecular species to arrange into complex architectures, has enabled a range of nanomaterials to be devised for drug delivery including liposomes,[3] porphysomes,[4] and polymeric micelles.[5] By exploiting self-assembly, reversibility can be engineered into self-assembled structures where the materials can be designed to respond to external (temperature, magnetic field, light, ultrasound) or endogenous (pH, enzymatic reaction, glucose, redox environment) stimuli,[6–12] thereby allowing for the release of therapeutic drugs. Self-assembled nanomaterials are therefore considered promising nanosystems to deliver drugs and biological macromolecules for therapeutic applications.[13]

Directed self-assembly, involving the spontaneous self-organization of molecules on a template,[14] has been used in the bottom-up synthesis of a broad range of drug delivery vehicles such as hollow capsules[15,16] and liposomes.[17] Control over the assembled material properties in terms of size and rigidity can be achieved by judicious choice of the template, including solid (e.g., polystyrene[18] or gold[19] particles), porous (e.g., silica[20] or calcium carbonate[21] particles), or liquid (e.g., emulsions[22–24]) templates. In addition, the type of template can influence the loading of therapeutics. For example, oil-in-water (O/W) emulsion templates can dissolve large quantities of hydrophobic molecules (drugs or imaging reagents) within the oil phase.[25,26]

Besides material physical properties, the surface chemistry of the assembled materials can influence their interaction with proteins and biomolecules, which ultimately determines the fate of the materials in vivo.[27,28] Using poly(ethylene glycol) (PEG)-based surface motifs on nanoparticles[29] and hollow capsules[9] , for example, allows for long blood circulation lifetimes in vivo and stealth-like behavior with regards to cellular association, respectively. Therefore, the

directed self-assembly of PEG-based molecules on O/W emulsion templates offers interesting possibilities for producing hybrid PEG/hydrophobic nanosystems that exhibit high loading capacities of therapeutics with low-fouling properties.

Herein, we investigate the interfacial self-assembly of metal–phenolic networks (MPNs) (involving metal-crosslinked polyphenolic films) on the liquid–liquid interface of O/W emulsions for potential use as a therapeutic nanomaterial. Our focus is the development of MPN–emulsion systems as responsive, biodegradable materials, and MPNs are chosen as the self-assembling material owing to their versatility and negligible cytotoxicity.[30] Ultrasonication of oleic acid (OA) mixtures in water generated nanoemulsions of ~100–250 nm in diameter, to which a synthetic polyphenol comprising PEG was self-assembled and crosslinked by Fe^{III} to form a surface MPN film on the emulsion phase. The PEG coating provided a low-fouling barrier on the emulsion in the presence of serum proteins, while also preventing coalescence and leakage of embedded cargo. The coated emulsions have an in vivo circulation half-life of ca. 50 min and are biodegradable. Importantly, by using MPNs as the protective barrier on the emulsion, we imparted pH-responsiveness for cargo release upon cellular internalization. When a model drug (doxorubicin) is loaded within the emulsion, this pH-responsiveness led to a potent cytotoxicity to human breast cancer cells.

2. Results and Discussion

2.1. Fabrication of Emulsion Metal–Phenolic Networks

OA emulsions were obtained by ultrasonic emulsification of a 0.03% OA (v/v) mixture in water, which is efficient for producing emulsions with diameters of suspended droplets of less than 200 nm.[31] Upon sonication, the mixture turned opaque, depending on the volume fraction of OA (see digital photograph in **Figure 1**). The resulting emulsions, with an average diameter of ~150 nm, as determined from dynamic light scattering (DLS) measurements (**Figure 2**A), were stable for several hours. The water/OA emulsion was then used as a template for the interfacial self-assembly of MPNs. For MPN formation, phenolic moieties were chosen as ligands to coordinate to the Fe^{III} ions.

A PEGylated ligand was chosen to endow low-fouling properties to the emulsion. The phenolic moieties were incorporated by modifying 8-arm-PEG-polyphenol with 5-hydroxydopamine via amide bonds, where the terminal galloyl motifs can form coordination complexes with Fe^{III} centers.[30] All eight PEG end-groups were conjugated to galloyl groups, as determined by ^{1}H NMR (Figure S1).

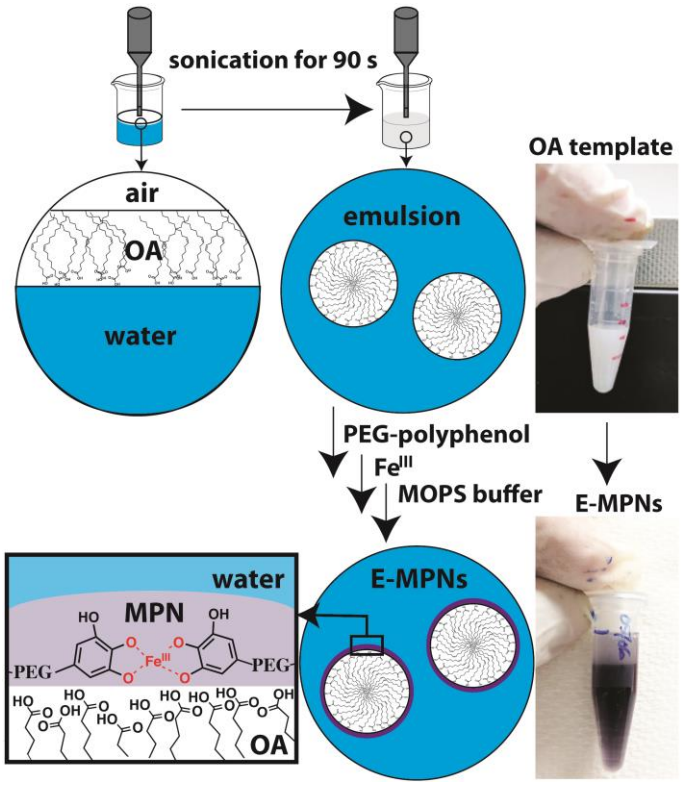

Figure 1. Schematic of the deposition of PEG-polyphenol MPNs on oleic acid (OA) emulsions (E-MPNs). The chemical structure of PEG-polyphenol is given in Figure S1 (Supporting Information). Digital photographs show the change in dispersion color after the formation of E-MPNs for a 0.3% OA/H_2O (v/v) system.

PEG-polyphenol was added to the OA emulsion and incubated for 20 min on a rotary wheel before addition of $Fe^{III}Cl_3 \cdot 6H_2O$, and subsequent raising of the pH to 8.0 with 3-(N-morpholino)propanesulfonic acid (MOPS) buffer (see Figure 1). We refer to this product as emulsion MPNs (E-MPNs). The resulting dispersion was deep purple, indicating successful chelation of Fe^{III} by the phenolic moieties on the PEG-polyphenol. We infer that the primary chelation is between galloyl moieties and the Fe^{III} centers,[32] though there could be some coordination with the carboxylate groups of OA. However, in the absence of PEG-polyphenol (i.e.,

only OA and Fe^{III}), the OA emulsion phase quickly coalesced with no associated change in color, suggesting that the Fe^{III} ions may have caused enhanced interaction between the OA emulsion droplets. This indicates that the metal–phenolic coordination is the driving force for E-MPN formation.

The product E-MPNs were purified from excess starting material by elution through a NAP10 silica column. DLS analysis of the product E-MPNs revealed a size distribution centered at 180 ± 70 nm; in contrast, the OA template has a size distribution centered at 150 ± 58 nm (Figure 2A). This change in hydrodynamic size is likely a consequence of the changed surface properties of the emulsions after deposition of MPNs. The size distribution of the E-MPNs was further determined by transmission electron microscopy (TEM); the resulting size distribution closely resembled the DLS size distribution of the OA template (Figure 2A). Atomic force microscopy (AFM) analysis was performed on the E-MPNs deposited on a silicon wafer and revealed that the E-MPNs have a diameter of ~200 nm (Figure 2B and Figure S2), corresponding to a slight increase in size from the size (~180 nm) determined by DLS. This slight increase in size is likely a consequence of the deformation of the soft internal OA phase upon evaporation of the solvent during sample preparation.

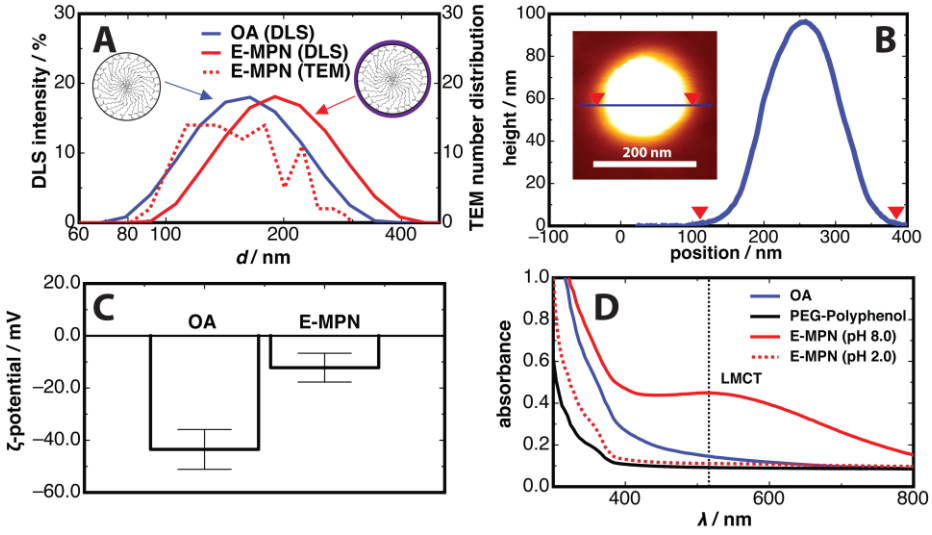

Figure 2. A) DLS size distributions of OA emulsions, and DLS and TEM size distributions of E-MPNs. B) AFM image of an E-MPN with accompanying line profile. C) ζ-potentials of OA emulsions and E-MPNs. D) UV-Visible absorption spectra of OA, PEG-polyphenol, and E-MPNs at pHs 8.0 and 2.0.

The OA templates have a highly negative ζ-potential of about −45 mV (Figure 2C), likely due to the exposed carboxylate groups of the fatty acid chains (Figure 1). This ζ-potential reduced to about −10 mV after the self-assembly of the MPNs. UV-Visible absorption spectra of the E-MPNs at pH 8.0 (Figure 2D) showed the presence of a ligand-to-metal charge transfer (LMCT) band at 520 nm, which was absent in the individual spectra of OA and PEG-polyphenol. This suggests a bis- and tris-type coordination between the Fe^{III} and the PEG-polyphenol ligands in the E-MPNs.[30] Furthermore, this LMCT band disappeared at pH 2.0, indicating disassembly of the MPNs at that pH. Together, these data indicate the successful formation of E-MPNs from the self-assembly of MPNs at the water/OA emulsion interface.

The dispersity of the E-MPNs was further confirmed by high-angle annular dark-field scanning transmission electron microscopy (HAADF-STEM); a significant difference in contrast between the E-MPNs and the background could be observed (**Figure 3**A). This highlighted the presence of heavy metal atoms (i.e., Fe^{III}), further confirmed by energy-dispersive X-ray spectroscopy elemental mapping (Figure S3). The Fe elemental pattern matched that of carbon within an E-MPN. Comparative TEM images of the OA templates and the E-MPNs, Figure 3B and C, respectively, showed very little contrast for the OA. This was expected for a hydrocarbon phase, whereas the E-MPNs appeared as solid black species due to the presence of Fe^{III}. The diameters of the E-MPNs obtained from both TEM and HAADF-STEM analyses corroborated the data obtained from DLS and AFM in Figure 2A and B, respectively. Furthermore, the TEM images showed that the E-MPNs are dispersed (i.e., little aggregation), possibility a consequence of the retention of a mildly negative ζ-potential post-MPN formation (Figure 2C).

To assess whether the film directly assembles on the liquid–liquid interface or is slightly embedded within the OA phase, owing to the amphiphilic nature of PEG, both the OA templates and E-MPNs were subjected to electrochemical measurements. The OA emulsions and E-MPNs were drop-cast onto a glassy carbon electrode, and following air-drying of the coated electrode, cyclic voltammetry (CV) profiles were recorded in the potential region ranging from −500 to +900

mV. As observed from the CV profiles in Figure 3D, both the OA emulsions and E-MPNs exhibited redox responses with distinct oxidation and reduction regions.[33] However, the E-MPNs had a significantly more pronounced oxidation response, which was attributed to the irreversible oxidation of the galloyl moieties on the PEG-polyphenol ligand.[33] This result suggests that the surface of the E-MPNs is functionalized with PEG-polyphenol moieties, as consistent with the reduction in ζ-potential observed (Figure 2B).

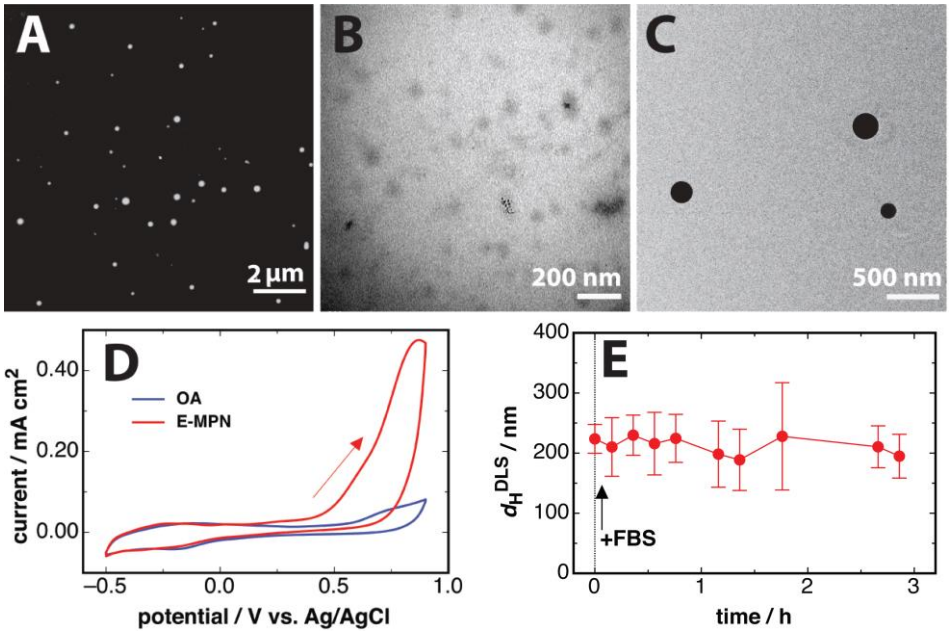

Figure 3. A) HAADF-TEM image of E-MPNs. TEM images of B) an OA emulsion and C) E-MPN particles. D) Cyclic voltammograms of OA emulsions and E-MPNs recorded under static conditions and at a scan rate of 5 mV s^{-1}; the arrow indicates the direction of the scan. E) DLS hydrodynamic size measurements of E-MPNs in PBS buffer (pH 7.4, 10 mM) at 23 °C with FBS added after the initial measurement (1% (v/v) FBS final mixture). Addition of FBS is indicated by the arrow. Error bars indicate standard errors.

By using a PEGylated polyphenol as the MPN ligand, the E-MPNs are expected to display low-fouling properties, which is a key requirement for drug delivery applications where a low level of nonspecific interactions with blood components is desirable.[34,35] The fouling of E-MPNs by serum proteins was determined by time-staggered DLS measurements,[36] with an aliquot of fetal bovine serum (FBS) added (to make a 1% FBS solution (v/v) in phosphate-buffered saline (PBS)) after the first measurement. Subsequent measurements were performed over 3 h. Only minor variations in the hydrodynamic diameter of the E-MPNs were observed (Figure 3E), along with a small reduction

in ζ-potential (Figure S4), suggesting that the colloidal stability of the E-MPNs was not compromised upon adsorption of serum proteins. UV-Visible absorption spectra of E-MPNs in buffer and of E-MPNs in buffer in the presence of FBS (Figure S5) both showed the presence of an LMCT band at 520 nm, demonstrating that the PEG-polyphenol remained chelated by Fe^{III} in the presence of serum proteins. Furthermore, the MPN coating on the OA emulsions provided long-term stability of the emulsion phase. After 9 days of incubation in MOPS, the E-MPNs maintained a consistent size distribution, whereas the OA templates coalesced into larger aggregates with time (Figure S6).

2.2. Cellular Association and In Vivo Biodistribution

We next examined the resistance of the E-MPNs to nonspecific cellular association. Fluorescently labeled E-MPNs (PEG-polyphenol labelled with Alex Fluor 488) were incubated with MDA-MB-231 human breast cancer cells, and cell association was evaluated by flow cytometry. A series of time points spanning from 2 to 18 h of incubation was studied (**Figure 4**A). The percentage of cells associated with E-MPNs steadily increased from ~10% after 2 h to ~45% after 18 h. This level of association indicates some nonspecific interactions with the MDA-MB-231 cells, but may allow for an increased circulation lifetime before cell uptake. A pharmacokinetic study was performed in healthy mice (C57BL/6) by monitoring the trace of fluorescently labeled E-MPNs in the bloodstream post-intravenous injection (Figure 4B). Figure 4B shows the blood clearance as a function of time; the blood circulation half-life of the E-MPNs was calculated as 48.3 ± 23.4 min. This circulation half-life is shorter than that of other PEG particle systems.[37] However, other than the type of particles, particle properties such as rigidity, surface chemistry, and density can affect the blood circulation.[38,39] Specifically, these properties affect cellular uptake and possibly the nature of the protein corona,[40] which together can alter blood clearance.

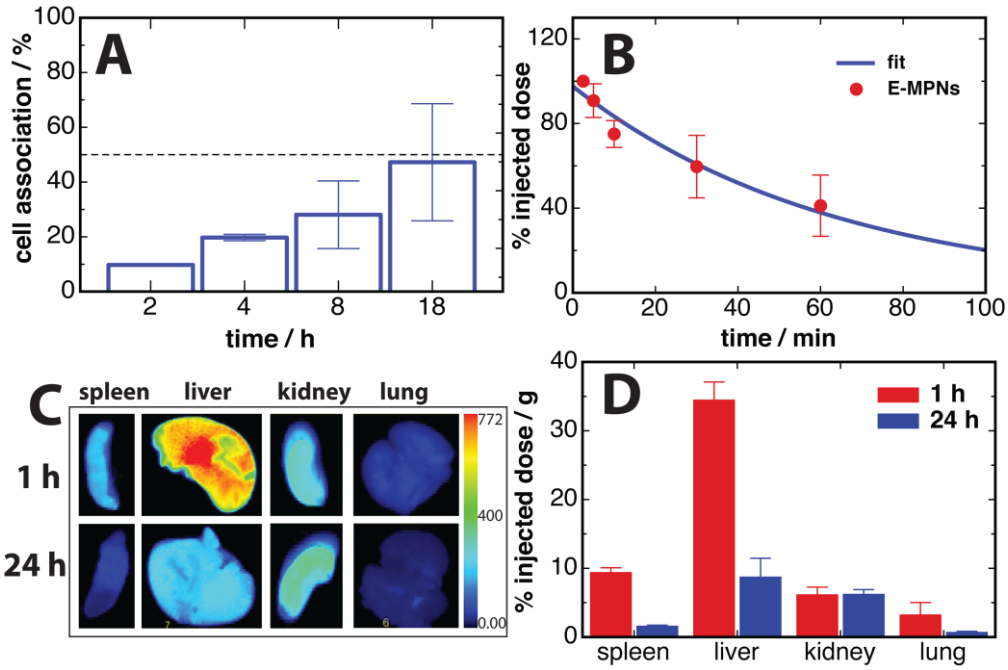

Figure 4. A) Cell association of E-MPNs with MDA-MB-231 breast cancer cells at a cell-to-particle ratio of 200:1. B) In vivo blood clearance of E-MPNs after intravenous injection, along with corresponding fit (see Supporting Information). C) Fluorescence detected in organs after 1 and 24 h post IV injections of fluorescently labeled E-MPNs. D) Quantification of fluorescence (calculated as the fluorescence intensity divided by the weight of the organ) in organs post IV injection of E-MPNs.

Characterizing the biodistribution of new nanomaterials is important for evaluation of their safety and determination of specific organ accumulation.[41] There are many parameters that influence the biological fate of emulsions in vivo, including size, oil phase, and the emulsifying agent (if used)[26] To examine the in vivo biodistribution of the E-MPNs, a known concentration of near-infrared label (Cy5- and Cy7)-loaded E-MPNs was intravenously injected into healthy mice. The animals were sacrificed at 1 and 24 h post-injection, and the organs were extracted to measure fluorescence intensity (Figure 4C). To account for the different weight of the organs, the normalized fluorescence intensity data are also shown in Figure 4D. At 1 h post-injection, the E-MPNs primarily accumulated in the liver (Figure 4C and 4D), with smaller amounts detected in the spleen, kidneys, and lungs. Interestingly, at 24 h post-injection, most of the E-MPNs were eliminated from the spleen, liver, and lungs, with only about 1, 10, and 0.5% remaining, respectively, indicating that the particles are biodegradable in these organs over time. This property is likely related to the stability of the MPN coating with pH[9,30] and the metabolism of fatty acids in the liver (i.e., OA)[42].

All animals survived the study—mice were active and showed no signs of lethargy or ill health after being dosed with known quantities of E-MPNs. These data show that the E-MPNs are nontoxic to healthy mice at the injected concentrations studied and that they preferentially accumulate in the liver, where they are biodegradable with time. The administration of other lipids has been associated with adverse side effects, but this is primarily in the form of nutrition rather than in the case of small-volume injections of emulsions for drug delivery.[43]

2.3. Anticancer Drug Encapsulation and Cell Viability Test

A key advantage of using an emulsion hydrophobic liquid phase as a template for MPN self-assembly is the possibility to load hydrophobic molecules such as hydrophobic drugs. This concept was examined by loading doxorubicin (Dox), a model anticancer drug, within the OA template. Dox was first mixed with the H_2O/OA mixture prior to sonication, thus allowing Dox to encapsulate within the OA phase upon sonication (Figure S7).[44] Following the deposition of MPNs, the same purification procedures were followed, with excess Dox removed by elution through a NAP10 silica column. After raising the pH of the dispersion (MOPs buffer, pH 8.0), the final Dox-loaded E-MPN dispersion was dark purple in comparison to a dark red Dox solution at the same pH, thus indicating successful crosslinking of the PEG-polyphenol ligands by the Fe^{III} centers. DLS was performed on the purified Dox-loaded E-MPNs; the size distribution was similar to that of the original OA template centered at 200 ± 110 nm (**Figure 5**A). This result indicated that the presence of Dox in the pre-sonicated water/OA mixture did not affect the size of the resulting emulsion templates or the effective deposition of MPNs on the drug-encapsulated template. The dispersity of the Dox-loaded E-MPNs was assessed by TEM (Figure 5B), which confirmed the particle size measured by DLS.

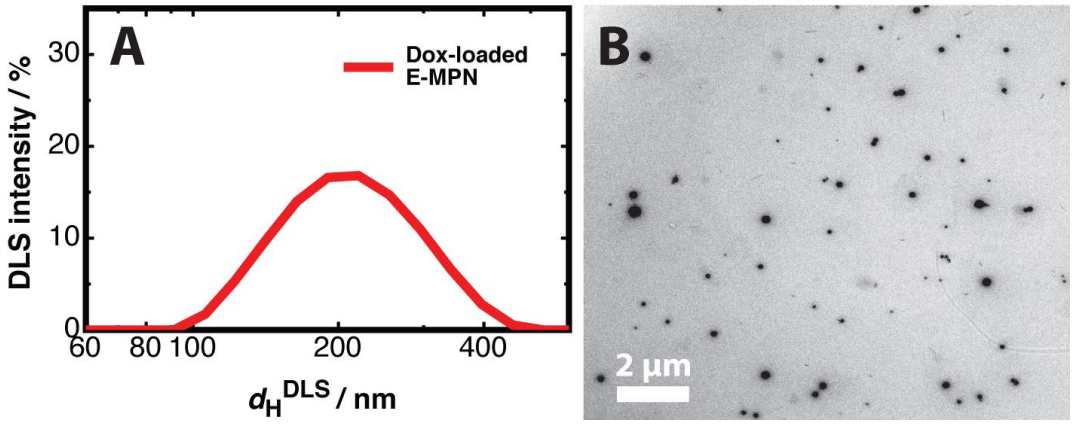

Figure 5. A) DLS intensity distribution and B) TEM image of Dox-loaded E-MPNs.

The concentration of Dox within the Dox-E-MPNs was determined by fluorescence measurements (excitation wavelength, λ_{ex} = 488 nm, emission wavelength λ_{em} = 595 nm) against a standard curve of Dox solutions in the same buffer at incremental concentrations (Figure S8). The result indicated that the purified Dox-loaded E-MPN dispersions had a concentration of ~16 µg mL^{-1}, which corresponded to ~10% loading efficiency based on the initial amount of Dox in the pre-sonicated solution. The mass dissolved in the pre-sonicated solution was varied, but with no corresponding change in the amount encapsulated. This observation indicated that we reached a limit in the amount of Dox that could be encapsulated within the E-MPN system. From nanoparticle tracking analysis (NTA), we deduced the number of particles per unit volume, and subsequently that the drug loading of each particle was ~5.3 fg of Dox, which was about the same as that observed for emulsion-templated polydopamine capsules that are about 5 times larger than the E-MPN particles.[45] Further comparison between the E-MPN particles prepared herein and other MPN-based particle systems of similar diameters reveals that the E-MPN particles have a drug loading capacity that is about 10 times greater.[29] This result indicates that our method provides a suitable approach to entrap a high concentration of hydrophobic therapeutics within an emulsion.

Given that the self-assembled E-MPNs are crosslinked via coordination bonds between Fe^{III} and the PEG-polyphenol galloyl groups, the stability of the E-MPNs is expected to be pH-dependent due to the stoichiometric transitions of the PEG-polyphenol–Fe^{III} complexes between tris-, bis-, and

mono-coordinations.[9,30] To assess the pH stability of Dox-loaded E-MPNs, the latter were incubated at pHs 7.4 (i.e., physiological pH) and 5.0 (i.e., cell internalization pH) at 37 °C within a spincolumn with a dialysis membrane of a cutoff of 30 kDa (see Figure S9). Over time, small aliquots of the external supernatant solution were taken for UV-visible measurements and referenced against known amounts of Dox at the same pH. After withdrawal of an aliquot, the same volume of buffer was replaced into the external supernatant solution. UV-visible analysis revealed that the Dox-loaded E-MPNs exhibit a pH-responsiveness for drug release (**Figure 6**A). At pH 7.4 the release was significantly lower than at pH 5.0. Specifically, over the time course studied, ~10% of Dox was released at pH 7.4 compared to ~60% at pH 5.0. The result suggests that at pH 7.4, the E-MPNs remain crosslinked, hence retarding the release of the cargo, whereas at pH 5.0, crosslinking in the E-MPNs partially disassembles, resulting in the release of Dox.

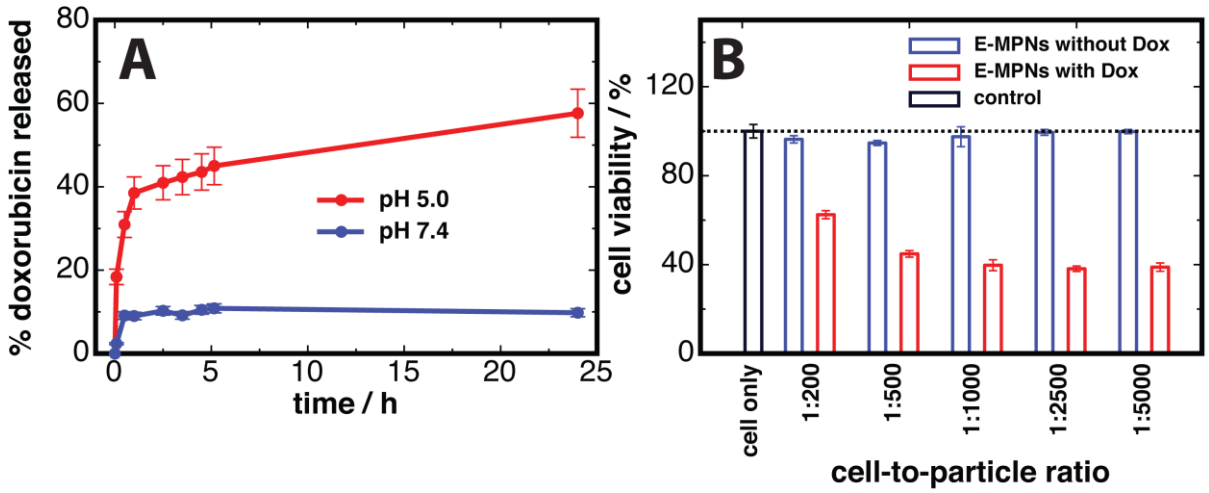

Figure 6. A) Release of Dox from Dox-loaded E-MPNs as a function of time at pHs 5.0 and 7.4 at 37 °C. B) Cytotoxicity of E-MPNs and Dox-loaded E-MPNs against MDA-MB-231 cells as a function of cell-to-particle ratio after 48 h of incubation in complete medium with 10% FBS at 37 °C. A control "cell only" system is also shown. The data are shown as means ± standard deviations.

The cytotoxicity of unloaded E-MPNs and Dox-loaded E-MPNs against MDA-MB-231 cells was investigated using the 3-(4,3-dimethylthiazol-2-yl)-2,5-diphenyltetrazolium bromide (MTT) assay. Both the E-MPN and Dox-loaded E-MPN dispersions were standardized to the same particle concentration in Dulbecco's PBS, as quantified by NTA (Figure S10). The MTT assay (Figure 6B) showed that the cell viability was greatly reduced for the Dox-loaded E-MPNs, in comparison with

that observed for the unloaded E-MPNs, demonstrating a potent cytotoxicity of the Dox-loaded E-MPNs. This cytotoxicity is likely a result of the pH-dependent Dox release at cell internalization pH. Dox-loaded E-MPNs showed a higher or comparable cytotoxicity to free Dox at the same drug dosage (Figure S11), suggesting the uptake of nanoparticles by MDA-MB-231 cells. Interestingly, the cell viability with Dox-loaded E-MPNs reaches a plateau, which may indicate that the cell internalization of E-MPNs reaches a saturation point. Furthermore, in comparing the unloaded E-MPNs to the cell only system, it was observed that the E-MPNs exhibit no cytotoxicity even at cell-to-particle ratios of 1:5000. This suggests that E-MPNs could potentially be used for imaging systems, where cell cytotoxicity is undesirable.

3. Conclusion

We have reported the interfacial self-assembly of PEGylated MPNs on the liquid–liquid interface of oleic acid emulsions. The resulting coated emulsions, termed E-MPNs, were ~100–250 nm in diameter and stable in the presence of serum proteins, and displayed stealth-like behavior with regards to cell association and a blood circulation half-life of ca. 48 min in vivo. The E-MPNs mainly accumulated in the liver, but biodegraded after 24 h. Moreover, we demonstrated that a model anticancer drug, Dox, could be encapsulated within the E-MPN at a high loading capacity of ~5.3 fg of Dox per particle. The release of the drug was pH-dependent, a feature imparted by the use of the MPNs as the encapsulating layer. These drug-loaded E-MPNs exhibited a potent cytotoxicity to human breast cancer cells, demonstrating successful cell internalization and release of active drug. Our results highlight a straightforward, self-assembly strategy for generating low-fouling, emulsion nanomaterials with pH-triggered decomposition properties, which may have potential use in biomedical applications.

4. Experimental Section

Materials: 8-Arm-poly(ethylene glycol) succinimidyl succinate (8-arm-PEG-NHS, hexaglycerol core, M_W 10 kDa) was purchased from JenKem Technology (USA). OA, $FeCl_3 \cdot 6H_2O$, MOPS, 5-hydroxydopamine hydrochloride, PBS tablets, Dulbecco's PBS, triethylamine (TEA), anhydrous *N*,*N*-dimethyl formamide (DMF), anhydrous dimethyl sulfoxide (DMSO), deuterium oxide (D_2O),

cetyltrimethylammonium tosylate (CTAT), tetraethyl orthosilicate (TEOS), triethanolamine, and FBS were purchased from Sigma-Aldrich (St. Louis, MO, USA). Cyanine 5.0 (Cy5) NHS ester and Cyanine 7.0 (Cy7) NHS ester were purchased from Lumiprobe. Doxorubicin hydrochloride (purity 99%) was purchased from OChem Inc. (USA). All chemicals were used as received without further purification. High-purity water with a resistivity greater than 18.2 MΩ cm was obtained from a three-stage Millipore Milli-Q plus 185 purification system (Millipore Corporation, Billerica, MA, USA). The pH of all solutions were measured with a Mettler-Toledo MP220 pH meter. All aqueous solutions were filtered with a 0.45 μm syringe filter before use.

PEG-Polyphenol Synthesis: 8-Arm-PEG-NHS (10 kDa, 100 mg, 10^{-5} mol) and 5-hydroxydopamine hydrochloride (82.3 mg, 4×10^{-4} mol, 1:5 PEG terminal/5-hydroxydopamine molar ratio) were respectively dissolved in 1 and 0.5 mL of degassed anhydrous DMF. The two solutions were then mixed and degassed by argon bubbling. Subsequently, 66.5 μL (4.88×10^{-4} mol) of anhydrous TEA (1.2:1 TEA/5-hydroxydopamine molar ratio) was added. The mixture was stirred at 23 °C under argon for 12 h. The reaction mixture was purified by dialysis (3500 Da cutoff; Thermo Fisher Scientific, USA) for 3 days against 3 L of degassed Milli-Q water (adjusted to pH 3.5), followed by lyophilization to obtain PEG-polyphenol as a white powder. To fluorescently label the PEG polyphenol, 32 μL of AF488 cadaverine (1 mg mL^{-1} in anhydrous DMSO) was mixed with 8-arm-PEG-NHS solution, followed by addition of 5-hydroxydopamine and TEA as described above. Product characterization and modification efficiency were determined by ^{1}H NMR using a 400 MHz Varian INOVA system, with the sample dissolved in D_2O at 25 °C. Specifically, the efficiency of modification was determined by comparing the integral values of the methylene protons of PEG at δ = 3.65 ppm to the aromatic protons of 5-hydroxydopamine at δ = 6.35 ppm.

Fabrication of Emulsion Metal–Phenolic Networks: First, 1.5 μL of OA was added to Milli-Q (0.03% v/v mixture in 5 mL) in a 12 mL plastic tube, which was subsequently sonicated with a needle probe sonicator at 40% amplitude for 1.5 min (QSonica needle probe ultrasonicator, Newtown CT). The resulting emulsion was allowed to cool to 23 °C, before a 800 μL aliquot was

transferred via filtration (1.2 μm cutoff syringe filter) to an Eppendorf tube, and 400 μL of PEG-polyphenol (20 mg mL^{-1}) was added. The dispersion was then placed on a rotary wheel for 20 min. A freshly prepared solution of 283 μL of $FeCl_3 \cdot 6H_2O$ (6.60 mg mL^{-1}) was added, and the resulting dispersion was vortexed for 30 s. It was then transferred to a 12 mL tube, and 2 mL of MOPS buffer (10 mM, pH 8.0) was added. After addition of MOPS, the clear dispersion turned purple. The product-coated emulsions were purified using a NAP10 silica column with MOPS buffer (10 mM, pH 8.0) as eluent. Freshly prepared E-MPNs were used for each experiment. Stable E-MPNs could be synthesized by varying the volume fraction of OA from 0.03 to 0.3%. An OA volume fraction of 0.03% was used, unless otherwise stated.

For in vivo and in vitro studies, 10 μL of either Cy5 NHS ester (1 mg mL^{-1}) and Cy7 NHS ester (1 mg mL^{-1}), or Dox (mass dissolved in OA/Milli-Q solution) was dissolved in the pre-sonication mixture, allowing for internalization within the oil phase upon sonication. These loaded emulsions were subsequently coated with PEG-polyphenol and crosslinked by Fe^{III}, as above, and purified from excess starting materials by elution through NAP10 silica columns. Visual inspection showed clear band separation between E-MPNs and the dye (Cy5 or Cy7) and the drug (Dox). For the cell studies, samples were suspended in Dulbecco's PBS instead of MOPS buffer.

Cell Culture: Human breast cancer cell line MDA-MB-231 (ATCC, USA) was stored in Dulbecco's modified Eagle's medium, supplied with 10% FBS and 2 mM L-glutamine, at 37 °C with 5% CO_2 and 95% relative humidity.

Cell Association Study: MDA-MB-231 cells were seeded into a 24-well plate at a cell density of 8×10^4 cells per well. Subsequently, the seeded MDA-MB-231 cells were incubated overnight to allow cellular adhesion on substrates. AF488-labeled E-MPNs were incubated with cells at a capsule-to-cell ratio of 200:1 for different periods. After incubation, the cells were gently washed thrice with Dulbecco's PBS, collected by trypsinization, and analyzed with an Apogee A50-Micro flow cytometer (Apogee Flow Systems, UK). The degree of cell association of the capsules was

evaluated by using the percentage of cells that exhibited stronger fluorescence intensity than untreated cells.

Cell Cytotoxicity Study: MDA-MB-231 cells were seeded into a 96-well plate at a cell density of 1 × 10^4 cells per well. Subsequently, the seeded MDA-MB-231 cells were incubated overnight to allow cellular adhesion on substrates. Dox-labeled E-MPNs were incubated with cells at different capsule-to-cell ratios from 200:1 to 5000:1 for 48 h. The medium was then replaced with 100 μL of fresh medium containing MTT (0.5 mg mL^{-1}), and the cells were incubated for another 4 h at 37 °C. The resultant formazan was dissolved in 100 μL of DMSO in each well, and the absorbance at 570 nm was measured by an Infinite M200 microplate reader (Tecan, Switzerland).

In Vivo Studies: All procedures were conducted in accordance with the Australian National Health and Medical Research Council's published Code of Practice for the Use of Animal in Research, and experiments were approved by the Alfred Medical Research and Education Precinct (AMREP) Animal Ethics Committee (E/1625/2016/M). Mice were housed on a 12 h light/dark cycle with ad libitum access to food and water. To evaluate the blood clearance and biodistribution of E-MPNs in vivo, male C57BL/6 mice weighing around 25–30 g were first anaesthetized by ketamine (100 mg kg^{-1}) and xylazine (10 mg kg^{-1}) before intravenous (IV) injections of the testing materials (10 μL g^{-1}). To track the fluorescently labeled (Cy 7.5) E-MPNs in the bloodstream, aliquots (5 μL) of blood were taken at 2.5, 5, 10, 30, and 60 min, and 24 h post IV injections and spread on a glass slide prior to measurements with an Odyssey fluorescence scanner (LI-COR®). After 1 and 24 h, all mice were euthanized by an overdose of ketamine and xylazine. Organs i.e. liver, spleen, kidney, and lung were collected and weighed prior to measurements with an Odyssey fluorescence scanner.

Instrumentation: DLS and ζ-potential measurements were performed with a Malvern Zetasizer instrument fitted with a 4 mW He-Ne laser (633 nm). UV-Visible absorption and fluorescence emission profiles were obtained with an Infinite M200 microplate reader in triplicates. UV-Visible absorbance was measured between 350 and 800 nm, and fluorescence emission was measured between 515 and 800 nm, with excitation at 488 nm (Dox). AFM measurements were performed on

a JPK NanoWizard II BioAFM instrument, with Bruker RTESPA-300 cantilevers in tapping mode. The E-MPNs were deposited on piranha-cleaned silicon wafers and subsequently dried under a stream of nitrogen. Particle concentration and size were measured via NTA performed on a Malvern NanoSight NS400 instrument fitted with a 405 nm laser (65 mW output). Samples were diluted by ×50 in MOPS buffer (10 mM, pH 8.0) and injected into the capillary line under a flow rate of 50 μL min^{-1}, with images captured over 60 s for 5 separate periods. Particle tracking was subsequently averaged over the 5 time periods for particle concentration and size results. For transmission electron microscopy (TEM), 5 μL of the E-MPN suspension was placed on a copper grid and allowed to air dry. TEM images were acquired using a FEI Tecnai F20 instrument with an operation voltage of 200 kV. Electrochemical experiments under static conditions were performed using a MM510 potentiostat/galvanostat (MMates, Italy). For the CV measurements, a standard three-electrode electrochemical cell that comprised a glass carbon electrode (GCE) (diameter = 3 mm), a Pt wire, and Ag/AgCl (KCl) as the working, counter, and reference electrodes, respectively, was used. For all electrochemical measurements, 1 M Na_2SO_4 aqueous solution was used as the supporting electrolyte. The supporting electrolyte was deaerated by purging nitrogen for 30 min before each measurement. The OA templates or E-MPNs suspension was drop-cast onto the GCE and air-dried. Before each drop-casting procedure, the GCE was thoroughly polished using an alumina polishing kit and washed with ethanol. Cyclic voltammograms on the GCE were recorded in the potential region ranging from −500 to +900 mV. The scan rate was 5 mV s^{-1}.

Supporting Information
Supporting Information is available from the Wiley Online Library or from the author.

Acknowledgements
This work was conducted and funded by the Australian Research Council (ARC) Centre of Excellence in Convergent Bio-Nano Science and Technology (project no. CE140100036). This research was also supported by the ARC under the Future Fellowship scheme (F. Cavalieri, FT140100873). F. Caruso acknowledges the award of a National Health and Medical Research Council Senior Principal Research Fellowship (APP1135806). We acknowledge the Bio21 Advanced Microscopy facility and the Bioscience Microscopy Unit at The University of Melbourne.

We thank Dr. Tim Ryan for useful discussions and Mr. Paul Brannon for assistance with the microscopy analyses.

Received: ((will be filled in by the editorial staff))
Revised: ((will be filled in by the editorial staff))
Published online: ((will be filled in by the editorial staff))

References

[1] R. Toy, P. M. Peiris, K. B. Ghaghada, E. Karathanasis, *Nanomedicine* **2014**, *9*, 121.

[2] G. Chen, I. Roy, C. Yang, P. N. Prasad, *Chem. Rev.* **2016**, *116*, 2826.

[3] B. S. Pattni, V. V. Chupin, V. P. Torchilin, *Chem. Rev.* **2015**, *115*, 10938.

[4] Q. Zou, M. Abbas, L. Zhao, S. Li, G. Shen, X. Yan, *J. Am. Chem. Soc.* **2017**, *139*, 1921.

[5] H. Cabral, K. Kataoka, *J. Controlled Release* **2014**, *190*, 465.

[6] M. Grzelczak, J. Vermant, E. M. Furst, L. M. Liz-Marzán, *ACS Nano* **2010**, *4*, 3591.

[7] S. Mura, J. Nicolas, P. Couvreur, *Nat. Mater.* **2013**, *12*, 991.

[8] T. Suma, J. Cui, M. Müllner, S. Fu, J. Tran, K. F. Noi, Y. Ju, F. Caruso, *J. Am. Chem. Soc.* **2017**, *139*, 4009.

[9] Y. Ju, J. Cui, M. Müllner, T. Suma, M. Hu, F. Caruso, *Biomacromolecules* **2015**, *16*, 807.

[10] A. P. R. Johnston, G. K. Such, F. Caruso, *Angew. Chem.* **2010**, *122*, 2723; *Angew. Chem. Int. Ed.* **2010**, *49*, 2664.

[11] T. Liu, N. Zhang, Z. Wang, M. Wu, Y. Chen, M. Ma, H. Chen, J. Shi, *ACS Nano* **2017**, *11*, 9093.

[12] K. Zhang, H. Xu, X. Jia, Y. Chen, M. Ma, L. Sun, H. Chen, *ACS Nano* **2016**, *10*, 10816.

[13] A. Yahia-Ammar, D. Sierra, F. Mérola, N. Hildebrandt, X. Le Guével, *ACS Nano* **2016**, *10*, 2591.

[14] E. M. Furst, *Soft Matter* **2013**, *9*, 9039.

[15] L. L. Del Mercato, M. M. Ferraro, F. Baldassarre, S. Mancarella, V. Greco, R. Rinaldi, S. Leporatti, *Adv. Colloid Interface Sci.* **2014**, *207*, 139.

[16] Y. Ping, J. Guo, H. Ejima, X. Chen, J. J. Richardson, H. Sun, F. Caruso, *Small* **2015**, *11*, 2032.

[17] Y. Yang, J. Wang, H. Shigematsu, W. Xu, W. M. Shih, J. E. Rothman, C. Lin, *Nat. Chem.* **2016**, *8*, 476.

[18] Z. Zang, M. Wen, W. Chen, Y. Zeng, Z. Zu, X. Zeng, X. Tang, *Mater. Des.* **2015**, *84*, 418.

[19] H. Zhang, S. Nayak, W. Wang, S. Mallapragada, D. Vaknin, *Langmuir* **2017**, *33*, 12227.

[20] F. Nador, E. Guisasola, A. Baeza, M. A. M. Villaecija, M. Vallet-Regí, D. Ruiz-Molina, *Chem. - Eur. J.* **2017**, *23*, 2733.

[21] B. V. Parakhonskiy, A. M. Yashchenok, H. Möhwald, D. Volodkin, A. G. Skirtach, *Adv. Mater. Interfaces* **2017**, *4*, 1.

[22] C. Fornaguera, A. Dols-Perez, G. Calderó, M. J. García-Celma, J. Camarasa, C. Solans, *J. Controlled Release* **2015**, *211*, 134.

[23] T. Fotticchia, R. Vecchione, P. L. Scognamiglio, D. Guarnieri, V. Calcagno, C. Di Natale, C. Attanasio, M. De Gregorio, C. Di Cicco, V. Quagliariello, N. Maurea, A. Barbieri, C. Arra, L. Raiola, R. V. Iaffaioli, P. A. Netti, *ACS Nano* **2017**, *11*, 9802.

[24] M. Ma, H. X. Xu, H. R. Chen, X. Q. Jia, K. Zhang, Q. Wang, S. G. Zheng, R. Wu, M. H. Yao, X. J. Cai, F. Q. Li, J. L. Shi, *Adv. Mater.* **2014**, *26*, 7378.

[25] C. Lovelyn, A. A. Attama, *J. Biomater. Nanobiotechnol.* **2011**, *2*, 626.

[26] K. Hörmann, A. Zimmer, *J. Controlled Release* **2016**, *223*, 85.

[27] D. Pozzi, G. Caracciolo, A. L. Capriotti, C. Cavaliere, G. La Barbera, T. J. Anchordoquy, A. Laganà, *J. Proteomics* **2015**, *119*, 209.

[28] A. C. G. Weiss, K. Kempe, S. Fo, F. Caruso, *Biomacromeolcules* **2018**, *19*, 2580.

[29] Y. Dai, J. Guo, T. Y. Wang, Y. Ju, A. J. Mitchell, T. Bonnard, J. Cui, J. J. Richardson, C. E. Hagemeyer, K. Alt, F. Caruso, *Adv. Healthcare Mater.* **2017**, *6*, 1.

[30] H. Ejima, J. J. Richardson, K. Liang, J. P. Best, M. P. Van Koeverden, G. K. Such, J. Cui, F. Caruso, *Science* **2013**, *341*, 154.

[31] M. Jaiswal, R. Dudhe, P. K. Sharma, *3 Biotech* **2015**, *5*, 123.

[32] M. A. Rahim, K. Kempe, M. Müllner, H. Ejima, Y. Ju, M. P. Van Koeverden, T. Suma, J. A.

Braunger, M. G. Leeming, B. F. Abrahams, F. Caruso, *Chem. Mater.* **2015**, *27*, 5825.

[33] P. V. Cherepanov, M. A. Rahim, N. Bertleff-Zieschang, M. A. Sayeed, A. P. O'Mullane, S. E. Moulton, F. Caruso, *ACS Appl. Mater. Interfaces* **2018**, *10*, 5828.

[34] Z. Amoozgar, Y. Yeo, *Wiley Interdiscip. Rev. Nanomed. Nanobiotechnol.* **2012**, *4*, 219.

[35] S. K. Mann, A. Dufour, J. J. Glass, R. De Rose, S. J. Kent, G. K. Such, A. P. R. Johnston, *Polym. Chem.* **2016**, *7*, 6015.

[36] F. C. Giacomelli, P. Stepánek, V. Schmidt, E. Jäger, A. Jäger, C. Giacomelli, *Nanoscale* **2012**, *4*, 4504.

[37] J. Cui, R. De Rose, K. Alt, S. Alcantara, B. M. Paterson, K. Liang, M. Hu, J. J. Richardson, Y. Yan, C. M. Jeffery, R. I. Price, K. Peter, C. E. Hagemeyer, P. S. Donnelly, S. J. Kent, F. Caruso, *ACS Nano* **2015**, *9*, 1571.

[38] C. D. Walkey, J. B. Olsen, H. Guo, A. Emili, W. C. W. Chan, *J. Am. Chem. Soc.* **2012**, *134*, 2139.

[39] J. Sun, L. Zhang, J. Wang, Q. Feng, D. Liu, Q. Yin, D. Xu, Y. Wei, B. Ding, X. Shi, X. Jiang, *Adv. Mater.* **2015**, *27*, 1402.

[40] P. Bertrand, A. Jonas, A. Laschewsky, R. Legras, *Macromol. Rapid Commun.* **2000**, *21*, 319.

[41] Y. S. S. Yang, P. U. Atukorale, K. D. Moynihan, A. Bekdemir, K. Rakhra, L. Tang, F. Stellacci, D. J. Irvine, *Nat. Commun.* **2017**, *8*, 1.

[42] E. Jurado-Ruiz, L. M. Varela, A. Luque, G. Berná, G. Cahuana, E. Martinez-Force, R. Gallego-Durán, B. Soria, B. de Roos, M. Romero Gómez, F. Martín, *Mol. Nutr. Food Res.* **2017**, *61*, 1.

[43] K. Hippalgaonkar, S. Majumdar, V. Kansara, *AAPS PharmSciTech* **2010**, *11*, 1526.

[44] X. Zhang, X. Sun, J. Li, X. Zhang, T. Gong, Z. Zhang, *Pharmazie* **2011**, *66*, 496.

[45] J. Cui, Y. Wang, A. Postma, J. Hao, L. Hosta-Rigau, F. Caruso, *Adv. Funct. Mater.* **2010**, *20*, 1625.

Low-fouling, biodegradable oil-in-water emulsions with diameters of 100–250 nm are produced by the self-assembly of metal–phenolic networks at the interface of emulsions. The coated emulsions are stable and exhibit a high drug-loading capacity and offer promise as a therapeutic nanocarrier.

Keywords: Oil-in-water Emulsions

Q. A. Besford, Y. Ju, T.-W. Wang, G. Yun, P. Cherepanov, C. E. Hagemeyer, F. Cavalieri, and F. Caruso*

Title: Self-Assembled Metal–Phenolic Networks on Emulsions as Low-Fouling and pH-Responsive Particles